

# Wind fields in heterogeneous conifer canopies: parameterisation of momentum absorption using high-resolution 3D vegetation scans

Ronald Queck · Anne Bienert · Hans-Gerd Maas ·  
Stefan Harmansa · Valeri Goldberg ·  
Christian Bernhofer

Received: 14 June 2010/Revised: 13 May 2011/Accepted: 12 July 2011/Published online: 4 August 2011  
© Springer-Verlag 2011

**Abstract** Applications of flow models to tall plant canopies are limited, amongst other factors, by the lack of detailed information on vegetation structure. A method is presented to record 3D vegetation structure and make this information applicable to the derivation of turbulence parameters suitable for flow models. The relationship between wind speed, drag coefficient ( $C_D$ ) and plant area density (PAD) was experimentally investigated in a mixed conifer forest in the lower part of the Eastern Ore Mountains. Essential information was gathered by collecting multi-level high-frequency wind velocity measurements and a dense 3D representation of the forest was obtained from terrestrial laser scanner data. Wind speed dependence or streamlining was observed for most of the wind directions. Edge effects, i.e. the influence of the here not regarded pressure gradient and the advective terms of the momentum equation, are assumed to cause this heterogeneity. Contrary to the hypothetic shelter effect, which would reduce the drag on sheltered plant parts, the calculated profiles of drag coefficients revealed an increasing  $C_D$  with PAD (i.e. a dependence on canopy and plant structure).

**Keywords** Drag coefficient · Terrestrial laser scanning · Vegetation model · Momentum flux

## Introduction

Detailed knowledge of momentum transfer between forest stands and the atmosphere is essential not only for assessing storm damage risks but also for understanding exchange processes of energy and greenhouse gases. The momentum absorption is dominated by inhomogeneities such as step changes in stand height and forest clearings (Hasager and Jensen 1999). Wind fields and turbulence structure within canopies are highly variable and depend on the distribution and shape of roughness elements (Raupach and Thom 1981; de Langre 2008).

Intensive experiments to assess the complete mass balance of several forest stands have revealed that measurements at discrete points unsatisfactorily represent the heterogeneity of energy and mass exchanges (Aubinet et al. 2010), and a complementary flow modelling is needed. The application of turbulence closure models that describe wind fields in tall canopies is, however, limited by the parameterisation of plant architecture (Cescatti and Marcolla 2004). The implementation of a realistic 3D plant surface model is a prerequisite for the adequate simulation of wind fields and for making comparisons of measurements and model simulations.

Terrestrial laser scanning, as a technology for close range applications, has proven to produce reliable representations of forest stand structure (Aschoff and Spiecker 2004; Gorte and Pfeifer 2004; Pfeifer and Winterhalder 2004; Henning and Radtke 2006; Maas et al. 2008). A plant area density can be estimated from laser scanning data by

---

This article belongs to the special issue ‘Wind Effects on Trees’.

Communicated by J. Bauhus.

---

R. Queck (✉) · S. Harmansa · V. Goldberg · C. Bernhofer  
Institute of Hydrology and Meteorology, Technische Universität  
Dresden, Piennner Straße 23, 01737 Tharandt, Germany  
e-mail: ronald.queck@tu-dresden.de  
URL: <http://tu-dresden.de/meteorologie>

A. Bienert · H.-G. Maas  
Institute of Photogrammetry and Remote Sensing,  
Technische Universität Dresden, Helmholtzstraße 10,  
01069 Dresden, Germany

aggregation of the laser scanner data into a 3D voxel space (Henning and Radtke 2006) or by identifying stem sections (Lefsky and McHale 2008). The first method is to prefer for the use in numerical flow models, which run mostly on 3D grid structures.

The drag force  $F_D$  experienced by vegetation due to atmospheric motion represents the strongest influence of vegetation on simulated wind fields. Following the concept of Rayleigh, it is usually calculated from the projected area (here PAD), the kinetic energy of the moving air mass and a drag coefficient,  $C_D$  (e.g. Shaw and Schumann 1992; Kaimal and Finnigan 1994). The term  $C_D$  is an object-specific coefficient that accounts for the drag reduction by the streamline form of the object, the influence of surface texture and, to some extent, the effects of viscous drag forces (see also Mahrt et al. 2001).

It has been reported that the product of  $C_D \times PAD$  decreases within closed canopies due to sheltering (e.g. Thom 1971) and that  $C_D$  depends on wind speed due to the streamlining of elastic roughness elements (Raupach and Thom 1981; Brunet et al. 1994; Finnigan 2000), but it has also been stated that the importance of viscous boundary layers increases at low Reynolds numbers (Mahrt et al. 2001). Furthermore, a dependence of  $C_D$  on wind direction is caused by variations in object shape and object size exposed perpendicular to the streamlines (Monteith and Unsworth 2008).

Despite the complexity of the drag coefficient, it is common to apply a constant  $C_D$  in numerical flow models (e.g. Shaw and Schumann 1992; Groß 1993; Yang et al. 2006; Frank and Ruck 2008; Dupont et al. 2011). However, Sogachev and Panferov (2006) emphasise the sensitivity of the turbulence parameterisation in regards to the drag

coefficient. Arya (2001) designates  $C_D$  as the most uncertain parameter in making estimates of momentum fluxes. Typical values used for coniferous forest stands range from 0.1 to 0.4, and for models, a constant value of  $C_D = 0.2$  is often used.

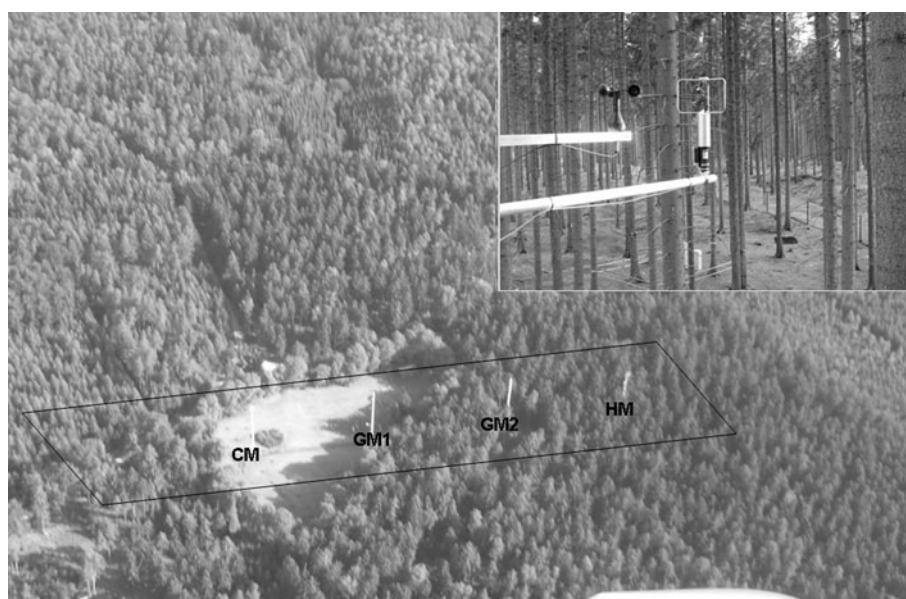
The aim of this study is to improve the representation of the vegetation in numerical models, as this is a major handicap for the calculation of realistic wind fields close to and within tall forests. The study uses data from two experiments called *WinCanop* and *TurbEFA*, and focuses on two questions: (1) How can we obtain a realistic vegetation model? (2) How can we parameterise the drag force acting on the vegetation?

## Materials and methods

### Study area

The Anchor Station Tharandter Wald (ASTW) has participated in various European projects to assess the carbon balance and is part of FLUXNET ([www.fluxdata.org](http://www.fluxdata.org)). It is located in the eastern part of a large forested area (60 km<sup>2</sup>), about 25 km southwest of Dresden, Germany (50°57'49" N, 13°34'01" E, 380 m a.s.l.) and comprises a forest stand that was seeded in 1887 and a clearing of 50 m × 90 m, called 'Wildacker' (see Fig. 1). Since 15 years, direct flux measurements are carried out at a 42 m scaffolding tower (HM) approximately 100 m east of the Wildacker. For this study, the investigated domain was aligned west to east according to the predominant wind direction and included the Wildacker. Most of the common features of the site were described by Feigenwinter et al. (2004) and Grünwald

**Fig. 1** Aerial photo with towers (courtesy of W. Junkermann, 31.07.2008) and the outlined model domain: *HM* indicates the permanent scaffolding tower (height 42 m), *GM1* and *GM2* are temporary scaffolding towers (40 m) and *CM* is a telescoping tower (30 m). The small photo in the upper right corner shows the southwest view from *HM* at a height of 8 m



and Bernhofer (2007); therefore, we have confined our description to stand features.

The main canopy is composed of 87% coniferous evergreen (72% *Picea abies* and 15% *Pinus sylvestris*) and 13% deciduous (10% *Larix decidua*, 1% *Betula* spp. and 2% others). The stand around HM is characterised by a dense canopy and an open trunk space with a sparse understory. In 2008, the mean canopy height ( $h$ ) around tower HM was estimated to be 31 m and the mean diameter at breast height as 36 cm. The determination of the single-sided plant area index (PAI) is based on a forest assessment from 1999 (including the harvest and analysis of 6 Norway spruces). Using continuous in-canopy radiation measurements (since 1996), the PAI was estimated to be  $7.1 \text{ m}^2/\text{m}^2$  in 2008.

Terrestrial laser scanning (TLS)

General method of TLS

A laser scanner consists of a range finder and a deflection unit. The range finder emits a pulsed or continuous laser signal and measures the distance to a surface. A deflecting unit is used to scan an object surface sequentially by laser pulses deflected by a rotating mirror (Vosselman and Maas 2010).

To ensure a complete scan of a large object, different laser scanner positions are necessary. The scans are merged into a single 3D representation of the object by using artificial tie points. The tie points are reflective objects (spheres and cylinders) placed on exposed positions at the site. By virtue of having at least 3 homologue tie points in each scan, the different scans can be referenced to one local coordinate system.

Laser scanner measurements are unorganised point clouds with several million points with  $x$ ,  $y$  and  $z$  coordinates. Digital terrain models (DTM) and digital surface models (DSM) of the above ground structures are generated (Kraus and Pfeifer 2001) using filtering and thinning techniques. Information about porous media-like forest canopies become feasible by aggregating the vast amount of measured points into 3D grid structures, so called voxel spaces. Each voxel holds statistical attributes (e.g. point density or point distribution parameters) of the enclosed volume (Bienert et al. 2010).

TLS measurements

In 2008, the forest stand around the clearing was scanned by TLS from 13 ground positions and additionally from the tops of towers HM and GM1 (at respective heights of 42 and 40 m). We applied two laser scanners with different specifications. First, a Riegl LMS-Z 420i laser scanner

(Riegl Laser Measurement Systems, Austria) with a distance accuracy of  $\pm 10 \text{ mm}$  and second, a Faro LSHE880 laser scanner (Faro Europe GmbH & Co. KG, Germany) with a distance accuracy of  $\pm 3 \text{ mm}$ . The ‘Riegl’ was adjusted to an angular resolution of  $0.1^\circ$  and the ‘Faro’ to  $0.036^\circ$ .

Plant area density

Defining 3D grid structure in a rectangular system with the coordinates  $x$ ,  $y$ ,  $z$ , the measured 3D point cloud can be transformed into a 3D voxel space as described in the following. On its way through the voxel space, a laser pulse penetrates different voxels before being reflected from the surface in a particular voxel. Some of the laser pulses, which go potentially in direction of a certain voxel, are being reflected by the vegetation in preceding voxels and do not reach the voxel.

Thus, the total of laser pulses in the direction of a voxel ( $N_{\max}$ ) is given by the laser pulses which are occluded before they reach the voxel ( $N_{\text{Occlusion}}$ ), hit a surface within the voxel ( $N_{\text{Hit}}$ ) or penetrate the voxel without interaction ( $N_{\text{Miss}}$ ) (see Fig. 2).

$$N_{\max} = N_{\text{Occlusion}} + N_{\text{Hit}} + N_{\text{Miss}} \tag{1}$$

Using these values, the likelihood of reflection ( $P$ ) is calculated for each voxel, yielding values between 0 and 1.

$$P(xyz) = \frac{N_{\text{Hit}}(xyz)}{N_{\text{Hit}}(xyz) + N_{\text{Miss}}(xyz)} \tag{2}$$

A similar method was also applied by Aschoff et al. (2006).

Within the single scans, shadows occur and objects behind other objects are not detected. The relative number of beams reaching a voxel can be used as a weighting parameter ( $w_i$ ) for the confidence of  $P$ .

Using different scan positions, a voxel can include laser measurements of different view directions. The combination of view directions reduces the number of hidden objects. The total reflection probability  $P_{\text{total}}$  combines the data from all of the scans using the confidence of the different  $P$ .

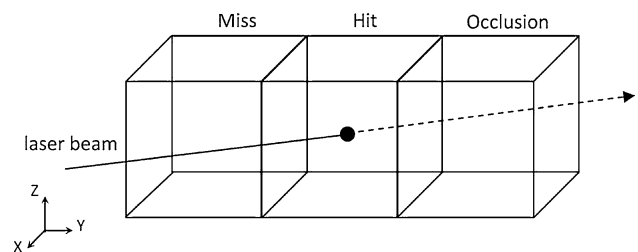


Fig. 2 Schematic ray tracing with a laser beam and an object point in a voxel space

$$P_{\text{total}} = \frac{\sum_{l=1}^n P_l \cdot w_l}{\sum_{l=1}^n w_l} \quad \text{with} \quad w_l = \frac{N_{\text{Hit},l} + N_{\text{Miss},l}}{N_{\text{max},l}} \quad (3)$$

where  $l$  is the index of the scan position and  $n$  the total number of scan positions. The term  $P_{\text{total}}$  is a measure for the surface density of each voxel and represents the PAD.

### Meteorological data processing

#### Wind measurements

The *WinCanop* experiment was carried out from June 2007 to November 2007. The setup of *WinCanop* was documented in Queck and Bernhofer (2010), thus we list only main features of the wind measurements here. The wind vector was measured by 13 ultrasonic anemometers/thermometers ('sonics') at tower HM (at heights of 0.2, 0.5, 2.0, 7.7, 13.3, 16.8, 21.6, 25.4, 27.8, 30.0, 33.0, 37.0 and 42.0 m).

During the *TurbEFA* experiment, intensive turbulence measurements were made along a transect over the clearing-forest interface from May 2008 to May 2009. The setup included four towers (up to 42 m) and five ground level positions (at 2 m). The wind vector was recorded at 32 positions in total. The presented work concentrates on the measured profiles at the tower HM, where seven sonics of type *USA-1* (Metek GmbH, Germany) were mounted at the heights of 2, 10, 20, 30, 33, 37 and 42 m.

The wind vector was synchronously sampled at 20 Hz in both of the experiments. The sonics were mounted vertically on booms at a distance of 2–3 m from the tower.

In post-processing, all raw data were rotated in one coordinate system and combined to half-hourly statistics. Several quality tests, including tests of spikes, stationarity and data gaps, were included in the routine and times with precipitation were excluded to avoid artefacts. In addition to the constraints with relation to data quality, we restricted the investigated dataset to near neutral cases (stability index between  $-0.1$  and  $0.1$ , based on measurements on HM at 42 m).

#### Momentum balance

In the following sections, the variables  $u$ ,  $v$  and  $w$  indicate the instantaneous values of the streamlined, lateral and vertical wind components, respectively; over bars denote time averages and a prime represents departures from time averages. The indices  $i$  and  $j$  indicate the three directions in space (i.e.  $u_1 = u$ ,  $u_2 = v$ ,  $u_3 = w$ ),  $t$  symbolises the time, the  $x_{i(j)}$  represent the spatial distances,  $\rho$  is the air density,  $p$  stands for air pressure and angle brackets denote spatial averages (see Raupach and Shaw 1982).

Within the forest canopy, under steady state conditions, neglecting the Coriolis force and buoyancy effect, the momentum equation is written as follows:

$$\frac{\partial \langle \bar{u}_i \rangle}{\partial t} = 0 = -\langle \bar{u}_j \rangle \frac{\partial \langle \bar{u}_i \rangle}{\partial x_j} - \frac{\partial \langle \bar{\tau}_{ij} \rangle}{\partial x_j} - \frac{1}{\rho} \frac{\partial \langle \bar{p} \rangle}{\partial x_i} - \frac{F_D}{\rho} \quad (4)$$

The terms on the right-hand side of Eq. 4 represent (from left to right) the advective transport, the kinematic flux tensor, the pressure gradient force and the drag force. Here,  $\bar{\tau}_{ij}$  is composed of the turbulent and molecular stresses as well as the dispersive flux (Wilson and Shaw 1977; Brunet et al. 1994), and  $F_D$  comprises the effects of the form drag and of the viscous drag. Like mentioned in the introduction, the concept of Rayleigh is commonly used to parameterise  $F_D$  in numerical models.

$$F_D = -\frac{C_D \cdot \text{PAD}}{P_m} \frac{\rho \cdot U^2}{2} \quad (5)$$

where  $U$  is a measure for wind speed (in the following generalised as velocity scale).

The shelter factor ( $P_m$ ) was termed by Thom (1971) and is defined as the ratio of the drag force on a solitaire plant part to the drag force on the same plant part placed in a plant community when applying an equivalent uniform wind.

Neglecting the advective transport, the pressure gradient, the molecular effects and the dispersive flux and assuming spatial representativeness, the stream-wise form of Eq. 4 reduces to the equilibrium between the kinematic stress gradient ( $\partial \overline{u'w'}/\partial z$ ) and the drag force (see Arya 2001, p. 376). Applying these assumptions and using Eq. 5 as a closure for  $F_D$ , the local drag area per unit volume ( $J$ ) can be defined on the basis of the momentum equation (e.g. Massman 1997; Cescatti and Marcolla 2004).

$$J(z) = \frac{C_D(z) \text{PAD}(z)}{P_m(z)} = \left| \frac{\partial \overline{u'w'}}{\partial z} \right| \frac{1}{U(z)^2} \quad (6)$$

According to meteorological conventions, the factor  $1/2$  on the right-hand side of Eq. 5 is included in the drag coefficient. An advantage of using the local drag area is the separation of parameters that describe vegetation structure from variables derived from wind measurements. Equation 6 is frequently used to calculate  $C_D$  from 3D wind measurements based on knowledge of PAD and estimations for  $P_m$  (Amiro 1990; Kerzenmacher and Gardiner 1998; Mahrt et al. 2001; Pinard and Wilson 2001; Cescatti and Marcolla 2004). In a first pragmatic approach, we used the mean values of PAD calculated from a volume of  $30 \text{ m} \times 30 \text{ m} \times 1 \text{ m}$  extending 30 m upwind from the sensor as a horizontal layer.

Velocity scale  $U$

The drag force experienced by vegetation is calculated from the loss of kinetic energy, which is represented by the squared wind speed  $U^2$  in Eq. 5. Common approaches use the squared arithmetic mean of the streamlined wind speed ( $\bar{u}^2$ ) for  $U^2$ . This has the consequence that, deep in the canopy where the mean velocity is low but turbulence levels remain high, the loss of kinetic energy is underestimated (Ayotte et al. 1999). An alternative averaging scheme replaces  $U^2$  with the averaged product of the absolute instantaneous wind intensity  $|U|$  and instantaneous longitudinal wind component  $u$  (see Cescatti and Marcolla 2004).

$$\overline{|U|u} = \sqrt{u^2 + v^2 + w^2} \cdot u \tag{7}$$

This approach emphasises the influence of wind speed fluctuations.

Results

Vegetation model

From 15 different scan positions, a combined point cloud of approximately 50 million surface points was created as a basis for analyses. The point cloud comprised the clearing and the neighbouring stands and had a dimension of approximately 120 m × 250 m × 44 m. For the outlined model domain, a DTM with a grid resolution of 0.5 m was generated from the lowest points of each grid cell (Fig. 3).

Under consideration of the scan positions, the point cloud was transformed into a voxel space with a voxel size of 1 m. Due to non-visible vegetation in very dense parts of the canopy, optical measurements tend to underestimate the PAD. Taking into account this uncertainty, we scaled the whole voxel space to match the known PAI around tower HM (PAI = 7.1 m<sup>2</sup>/m<sup>2</sup>).

Subtracting the DTM from the truncated voxel space and averaging in the  $y$ -direction over 60 m resulted in the 2D PAD distribution shown in Fig. 4.

Wind speed dependence of the local drag area

The following investigations were focused on winds from the west (wind sector: 255°–285°), as it is the most prominent wind direction. Using Eq. 6, the local drag area was calculated directly from the wind measurements. These values are expected to show a superposition of three effects. A decreasing local drag area with increasing wind speed is attributed to (i) a streamlined alignment of the canopy elements and (ii) a decreasing viscous boundary layers (as discussed in Mahrt et al. 2001). Furthermore, the drag force on plants depends on the square of the wind speed, i.e. the calculation of the arithmetic mean underestimates  $F_D$  that are caused by high wind speeds more than it overestimates  $F_D$  calculated at low wind speeds, which leads to (iii) an overestimation of local drag area at low mean wind speeds. The use of  $\overline{|U|u}$  (Eq. 7) as a velocity scale should circumvent at least the last problem.

Figure 5 compares  $\overline{|U|u}^{0.5}$  and  $\bar{u}$  derived from measurements at HM in the canopy space (at 22 m). For

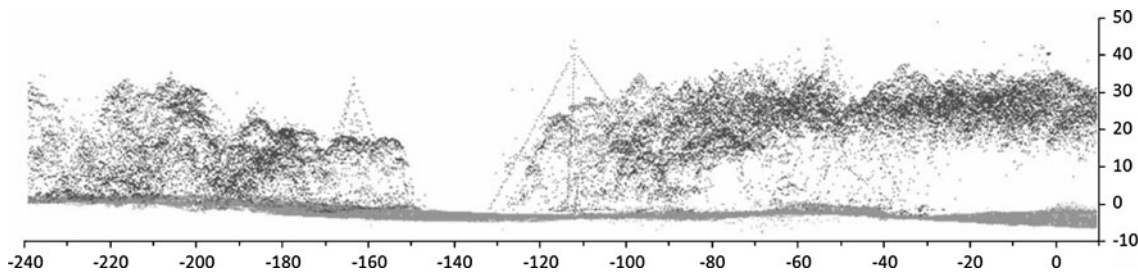
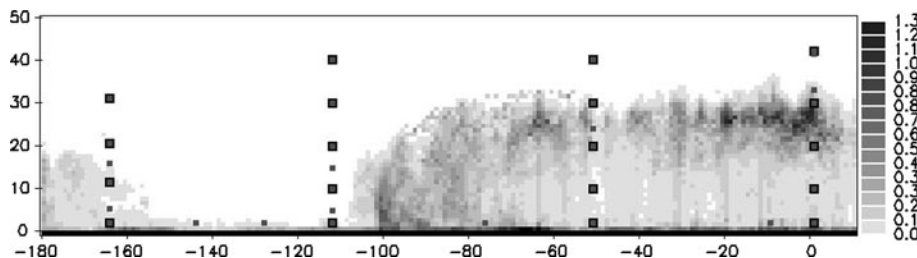
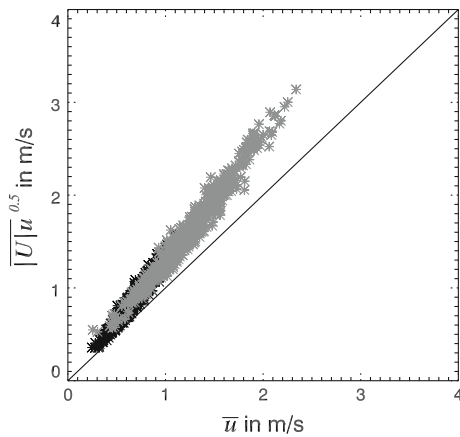


Fig. 3 Side view of the point cloud (points, thinned for presentation) and DTM (grey band, extracted on the basis of a raster size of 0.5 m), distances on the axes are given in m from the basis of tower HM

Fig. 4 Two-dimensional voxel space (of length  $x$  and height  $z$  in m) of mean PAD in m<sup>2</sup>/m<sup>3</sup>, derived by averaging the  $y$ -direction (depth) of the 3D voxel space. Small squares indicate anemometer positions





**Fig. 5** Comparison of velocity scales  $\overline{|U|u}^{0.5}$  and  $\bar{u}$  used for the calculation of  $J$  and  $C_D$  calculated from data measured at the permanent tower at heights of 25 m (black symbols) and 30 m (grey symbols); 1:1 relationship (black line)

constant laminar flow, Eq. 7 results in a 1:1 relation of the two velocity scales, however, any turbulence causes a higher  $\overline{|U|u}^{0.5}$ .

The dependence of  $J$  on wind speed at tower HM is shown in Figs. 6, 7 and 8 for the *WinCanop* and *TurbEFA* experiment. Thereby,  $J$  was calculated using gradients of different heights and with both velocity scales,  $\bar{u}^2$  and  $\overline{|U|u}$ . Figure 6 clearly shows  $J$  as a function of wind speed, especially, in the upper part of the canopy. The different gradients show also the height dependence of  $J$  which corresponds to PAD, and is discussed in the next subsection. The kinematic stress gradients measured in the dense canopy (around  $z = 20$  m) show large scatter and sometimes a change in the sign, which corresponds to a momentum transfer from the trunk space into the denser crown space. In general, the scatter of  $J$  is higher at lower wind speeds.

We also plotted  $J$  against the normalised velocity scales (Fig. 7). It is to mention that despite the restriction to neutral data, the normalised wind at one height covers a remarkable range of the  $x$ -axis, especially at the higher

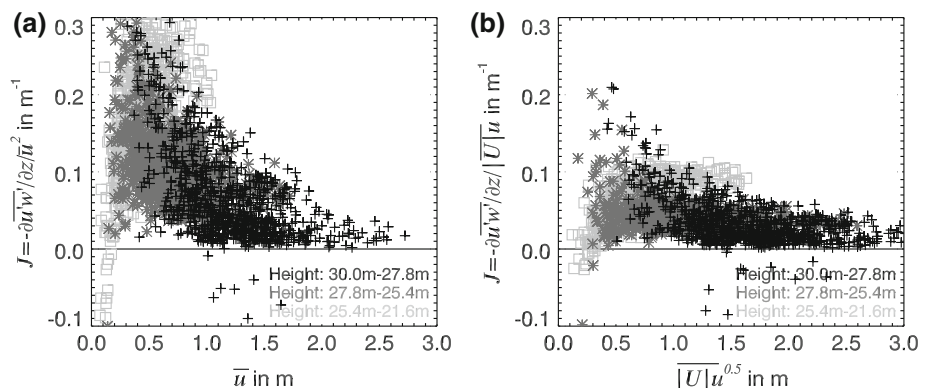
measurement levels. The plots in Figs. 6 and 7 show similar forms, though, the scatter of the points is reduced. This reveals that  $J$  is more a function of the vertical gradient of wind speed (i.e. the wind profile) than of the wind speed itself. Comparing the plots of the *WinCanop* and *TurbEFA* experiment confirms that, despite the different periods in time and changes in sensor positions, the point clouds have a similar shape. This indicates repeatable results. The data from *TurbEFA* show less scatter, which is attributed to the larger gradients examined.

Using  $\overline{|U|u}$  as a velocity scale eliminates the dependence on wind speed almost completely and reduces the scatter in  $J$  remarkably, which was also reported by Cescatti and Marcolla (2004). Apparently,  $\overline{|U|u}$  takes into account the increase of form and viscous drags in intermittent sequences with higher wind speeds during periods with weak winds on average. The remaining slight dependence of  $J$  on wind speed in the upper part of the canopy, between 30 and 25 m, is probably caused by streamlining due to bending of branches in the downwind direction. At the lower levels, no significant streamlining effect was observed. This may have been caused by the general lower wind speeds but also by the higher stiffness of older branches.

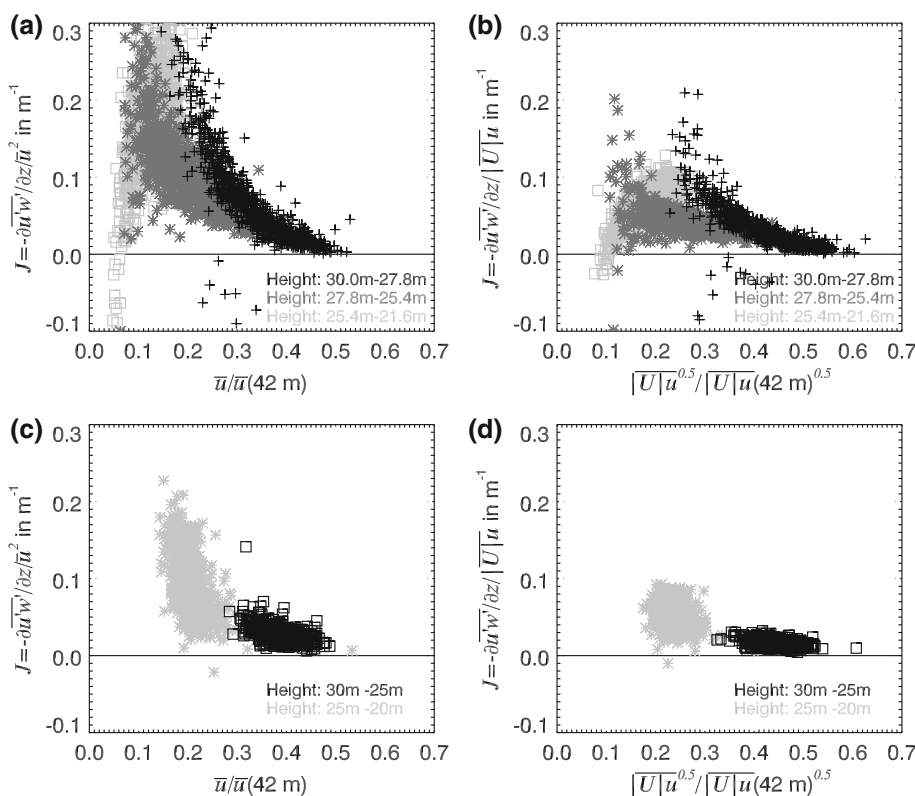
However, whilst a wind speed dependence of  $J$  is observable in all wind sectors from northeast over north to west, it seems to vanish completely under wind from the south and east (see Fig. 8). This inconsistency is considered in the discussion section.

Figure 9 provides a survey of the measured profiles and the results obtained at tower HM. The scatter plots of  $J$  in Fig. 9a show the slight dependence on wind speed discussed above and the median of  $J$  traces the PAD profile. The coefficient of variation is highest at the top of the canopy and in regions with a low PAD. The vertical profiles in Fig. 9b, c show a relative smooth course of the statistical means of the turbulent flow and no systematic instrument error or local influence of the vegetation is expected.

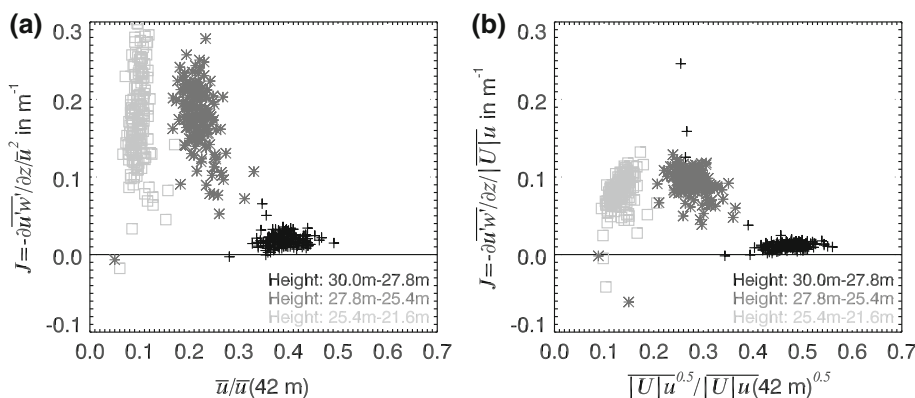
**Fig. 6** Local drag area  $J$ , calculated using the two different velocity scales, plotted versus the horizontal wind speed at tower HM for the west wind sector ( $255^\circ$ – $285^\circ$ ); plot a is calculated using  $\bar{u}^2$  and b using  $\overline{|U|u}$ ; the heights of the sensors are indicated within the charts (symbols with increasing height are: open squares, stars, crosses); measurements were collected during the *WinCanop* experiment



**Fig. 7** Local drag area  $J$  (on the y-axis) versus normalised horizontal wind speed at tower HM for the west wind sector (255°–285°), similar to Fig. 6. Plots **a** and **b** show measurements from 2007 taken during the *WinCanop* experiment and plots **c** and **d** show measurements from the *TurbEFA* campaign



**Fig. 8** Local drag area  $J$ ; similar to Fig. 7a, b, but for the southwest wind sector (195°–225°)



For the two normalised velocity scales  $\bar{u}$  and  $|\overline{U}|u^{0.5}$  in Fig. 9b, a maximum difference of about 10% was obtained at the heights between 25 and 30 m. The deviation between their profiles let expect that the linear relationship, shown in Fig. 5, is also a function of PAD and the turbulence intensity (Fig. 9c shows the kinematic shear stress as a measure of it). Both of them have a maximum within this region, too.

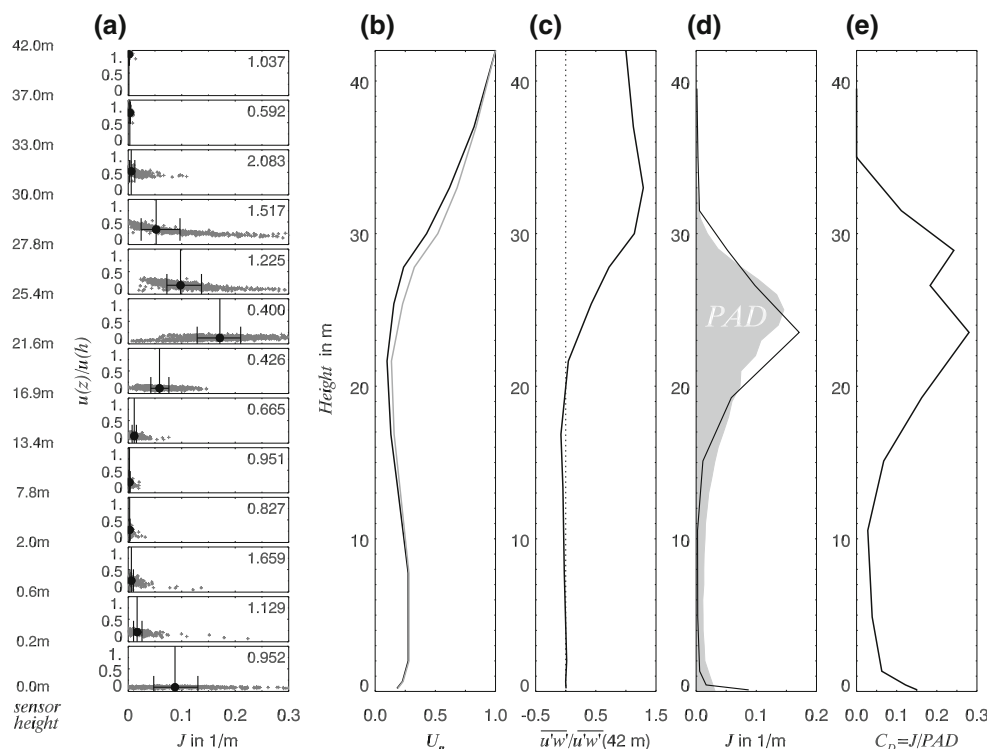
The derived local drag area (Fig. 9d) reaches its maximum value slightly below the densest part of the canopy. This causes a small irregularity in the profile of  $C_D/P_m$  (Fig. 9e). Considering the small gradients in trunk space, the derived drag coefficients should carry significant uncertainty (Pinard and Wilson 2001). However, besides a

small irregularity in the upper canopy, the profile of the calculated drag coefficients appears to be surprisingly smooth.

Is there a shelter effect?

Turbulence within the crown space is a composite of the wake production behind a multitude of object sizes (Cava and Katul 2008). The effect of turbulence generation (and momentum absorption) is not comparable to the sum of wakes behind single objects. The local drag area within closed canopies, the product of  $C_D$  and PAD, is therefore often related to a sheltering factor  $P_m$  (e.g. Massman 1987; Marcolla et al. 2003). Landsberg and Thom (1971) derived

**Fig. 9** Profiles at the permanent tower measured during the WinCanop experiment: **a** Normalised wind speed versus the calculated local drag area; the median of the point clouds is marked by a *black dot*; the *whiskers* show the 25th and 75th percentiles, and the coefficient of variation is printed in the *upper right corner* of each *plot*. **b** Normalised mean velocity scales ( $U_n$ ), i.e.  $\bar{u}(z)/\bar{u}(42\text{ m})$  in *black* and  $|\overline{U}|u^{-0.5}(z)/|\overline{U}|u^{-0.5}(42\text{ m})$  in *grey*. **c** Normalised kinematic shear stress. **d** Median of the *local drag area*, and PAD (without scale). **e** Drag coefficients (including the shelter coefficient)



a dependence on shoot density raised to a power of 0.43; Stewart and Thom (1973) found a  $P_m$  of 3.6 for a pine forest, and Massman (1987) estimated a value of 5.6 from the data of Li et al. (1985). Finally, Wood (1995) reports that trees sheltered by many others endure only 6–8% of the drag force of trees fully exposed to the same wind speed, which corresponds to a  $P_m$  between 12 and 16.

Contrary to these results, Fig. 10 shows positive correlations between  $J/PAD = C_D/P_m$  and PAD, indicating that drag force increases with PAD, which results in a  $P_m$  of less than one. Obviously, we are here facing another mechanism, and no shelter effect was observed in our experiments. Therefore, we neglect the  $P_m$  and set  $J/PAD = C_D$ . A regression of  $C_D$  on PAD in the wind sector 255°–285° gives  $C_D = 0.32 \text{ PAD} + 0.047$  (Pearson’s correlation coefficient is 0.797). Whereby, the values in the upper part of the canopy always occur above the regression line, which likely indicates an influence of the vertical advection. A positive regression is observed for all wind directions, whereas, the values of the parameter depend on wind direction. Figure 10b shows the results from wind sector 195°–225° again, which has a fetch of more than 10 h.

However, introducing a linear function in the closure for the drag force does not solve the problem, because it would also amplify the profile of  $C_D$  in Fig. 9e. To enhance the dependency on PAD, we plotted the data with logarithmic axes.

$$-\frac{F_D}{\rho} \frac{1}{\bar{u}^2} = \text{PAD}^a \cdot C_{D,r} \tag{8}$$

$$\log\left(-\frac{\partial u'w'}{\partial z} \frac{1}{\bar{u}^2}\right) = a \cdot \log(\text{PAD}) + \log(C_{D,r})$$

A linear regression yields an exponent  $a = 1.57$  for the PAD and a drag coefficient  $C_{D,r}$  of 0.327 for the wind sector 255°–285°. As this result is certainly specific to the vegetation structure of the investigated site, it needs to be verified by the analysis of further data before its application in a numerical flow model.

### Integrated canopy drag coefficient

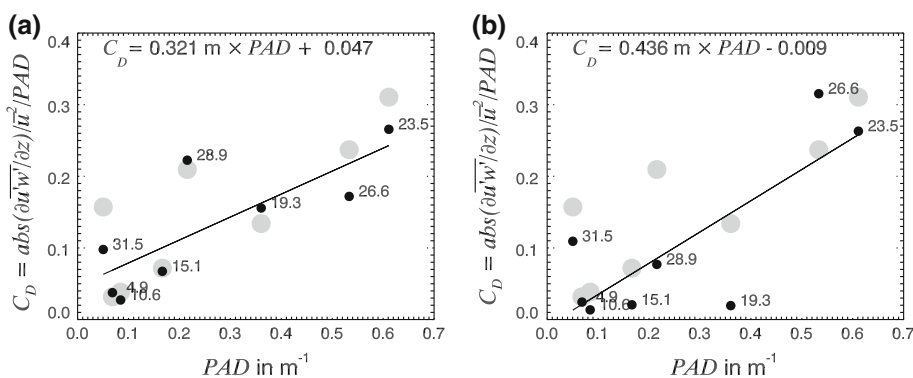
Drag coefficients that are derived from measurements within the canopy show large scatter and are still rarely reported, thus, we calculated averaged values and compared them with estimations for the whole canopy. Firstly, the derived  $C_D(z)$ , shown in Fig. 9e, were weighted with the distances between the measurements.

$$\overline{C_D} = \frac{\sum \Delta z \cdot C_D(z)}{h} \tag{9}$$

Secondly, an estimation of the height-averaged drag coefficient  $\overline{C_{Da}}$  was calculated from the Reynolds stress above the canopy and the wind profile, after Pinard and Wilson (2001).



**Fig. 10** **a**  $C_D$  versus PAD: *small dark dots* are calculated from the wind sector 255°–285° (the *black line* shows a regression of them); *bigger light grey dots* are ascribed to all wind directions and the numbers indicate the mean height in m of the underlying gradients, **b** same as **a** but for wind sector 195°–225°



$$\overline{C_{Da}} = \left( \int_0^h \text{PAD}(z) \frac{\overline{u(z)}^2}{\overline{u'w'}(42\text{ m})} dz \right)^{-1} \quad (10)$$

Both of the methods give plausible results (for the west wind sector:  $\overline{C_D} = 0.130$  and  $\overline{C_{Da}} = 0.132$ ) and they are very close to the values found in literature (e.g. Amiro 1990; Kerzenmacher and Gardiner 1998; Pinard and Wilson 2001). However, the magnitude of  $C_D$  depends strongly on wind directions (Fig. 11), and a range of 0.1–0.4 was covered by all measurements from tower HM.

**Discussion**

Reliability of the results

Applying an inverse approach to derive a vegetation parameterisation for numerical flow models from measurements, three questions must be addressed: (i) What is the influence of the not considered terms of the momentum

equation? (ii) Are the wind measurements and laser measurements representative? (iii) Which volume of vegetation influences the turbulence measured at a specific sensor position? Beside other considerations, these items are the main sources of uncertainty and cause a large part of the scatter and perhaps bias in the derived results.

(i) *Neglected terms of the momentum equation*

Equating the drag force with the vertical turbulent transport in the momentum equation neglects mainly the advective transport, the pressure gradient, the molecular effects and the dispersive transport.

The dispersive momentum transport arises from the spatial correlation of quantities averaged in time but varying with position (Raupach and Shaw 1982) and has been confirmed to be only about 1% of the Reynolds stress (Coppin et al. 1986). Molecular effects are also small and usually included in the drag coefficient. However, results of numerical models have revealed that advective transports and pressure gradients can yield a significant contribution to the momentum equation, especially in the vicinity of forest edges, where the flow is in the process of adjustment (Yang et al. 2006).

Dupont et al. (2011) described results from large eddy simulations (LES) for a pine stand with a clear trunk space (which is also the case for our site). For a fetch larger than 10 h, no significant contribution of the here neglected terms were calculated. However, for smaller fetches (4 h and 9 h), edge effects may occur. Then, the simulated local pressure gradient always adds a positive contribution to the momentum budget, which is compensated for by vertical advection in the upper crown space. However, the contribution of the vertical advection decreases with depth in the crown space and, in the case of a secondary wind maximum in trunk space, changes its sign in the lower crown space. Within the trunk space, the moment absorption should be mainly compensated for by the horizontal turbulent transport, the horizontal advection and the pressure gradient, which are not regarded in our calculations.

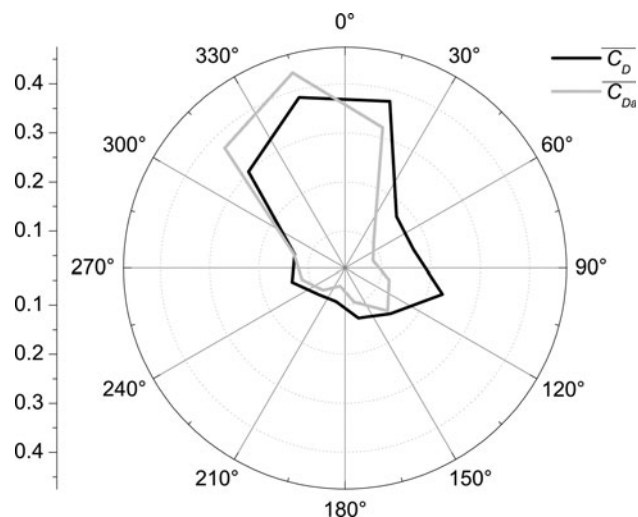


**Fig. 11** Spatial distribution of drag coefficients shown by the dependency of integrated drag coefficients on wind direction

Based on the results of Dupont et al. (2011), the error in the derived  $C_D$  made by the truncation of the momentum equation is estimated to be 10% in the upper ranges of the canopy but increases with the depth in the canopy. The results within the trunk space between 2 m and 17 m are not reliable.

### (ii) Representativeness of measurements

Besides instrument errors, we face methodical measurement problems in the spatial representativeness of wind measurements and penetrability of vegetation by a laser beam.

Equation 4 represents an area average over a horizontal plain intersecting numerous plants (Raupach and Shaw 1982). In distinction thereto, wind sensors are point measurements and are always subject to the flow through or around tree crowns; thus, a spatial mean is not achievable from direct measurements. The problem is depicted in the large vertical variability in wind direction shown in Fig. 12. At the top of the canopy (30 m), the half-hourly mean of the wind direction is in line with the measurements made at 42 m. Five metres below, at 25 m, the wind direction is clearly influenced by the trees around the sensor but at 20 m we observe another pattern again.

However, as most trees are vertically aligned, the problem seems far less pronounced for the vertical profiles of the mean wind and kinematic stress. The relative smooth course of the profiles in Fig. 9 indicates that the vertical transport is more homogenous than is the horizontal, which justifies the derivation of vertical gradients from point measurements.

Optical measurements of leaf area index (LAI) and PAD have a long tradition, and it is known that these measurements underestimate the impact of the clumping of vegetation elements on LAI. Commonly the concept of Beer–Lambert–Bouguer is used to describe the probability that light penetrates a volume or that it is absorbed by substances within the volume. However, this concept is only valid for media with low optical thicknesses such as gases. Dense canopies do not fulfil this restriction. The slightly different approach applied here was tested on a numeric canopy model with a given PAD and has shown a

better performance, but a validation with classical harvest methods is still needed. Nevertheless, we must take in account the increasing uncertainty that occurs with increasing PAD. The future application of morphological operations (dilatation and erosion) will give more information about shaded voxel and increase the reliability of the vegetation model (Bienert et al. 2010).

### (iii) Volume of influence

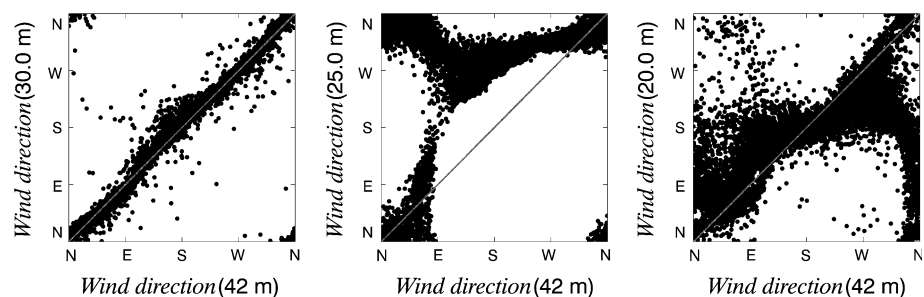
Finally, the mean angle of attack and the size of the volume for the spatial mean is to determine. It is possible to calculate the mean angle of attack during sweep events (see Cescatti and Marcolla 2004) or to use the tilt angle of half-hourly mean winds; however, these angles depend on wind speed, wind direction and measurement height. Further, it is to consider that vegetation elements close to the sensor probably have a stronger influence on the turbulent flow than do more distant ones. A further clarification of these problems is anticipated by detailed analysis of results from LES and Lagrange models. Having no general solution, we decided to use horizontal means of PAD.

### A variable drag coefficient?

The results of the experiments reveal a slight dependence of the local drag area on wind speed, i.e. a streamlining, as well as a non-linear dependence on PAD.

The velocity scale  $\overline{|U|u}$  seems to explain a major proportion of scatter in  $J$  and the wind speed dependency. However, for the application in a RANS model, no instantaneous wind speed is available, and a parameterisation of the effect of using  $\overline{|U|u}$  is necessary. Figure 6 indicates a reciprocal relationship of  $J$  to wind speed. Indeed, Wood (1995) discusses empirical formulas that lead to an increase of the drag force approximately in proportion to  $\bar{u}^{1.8}$  rather than to  $\bar{u}^2$ . Koizumi et al. (2010) derived  $C_D$  using stem deflection measurements and obtained patterns of the  $C_D$ –wind speed relationship that are similar to the results shown in Fig. 6. Fitting the power functions  $C_D = au^b$  to the data, they found exponents ( $b$ ) of wind speed in the range of  $-0.71$  to  $-0.91$ . This confirms our results for winds from the north

**Fig. 12** Half-hourly means of the wind direction at three different heights (30, 25 and 20 m) within the canopy space compared with measurements made at 12 m above the canopy (42 m), y-axes: sensors at different levels in the canopy, x-axes: sensor at the reference height (42 m)



and west (having a fetch of 3.5 *h*), for which a value of  $b = -0.8$  would fit best. However, we could not observe a dependence of  $J$  on winds from south (having a fetch of more than 10 *h*). This leads to the suggestion that edge effects are important for wind dependence of  $J$ . The measured vertical wind speed and the results of Dupont et al. (2011) indicate a serious influence of vertical advection (vertical advection would increase with the wind speed, i.e. the drag force, but not the gradient in kinematic stress).

The large variation of the  $C_D$  at low wind speeds (see Fig. 6) was also observed in the results of Koizumi et al. (2010), using a completely different approach to derive the  $C_D$ . However, to date no explanation of this behaviour could be found. Concerning these uncertainties, we recommend using  $\overline{|U|u}$ , or, if this term is not available, neglecting the wind speed dependence of  $C_D$  and using  $\bar{u}^2$  for the present.

The results for the dependence of the  $C_D$  on PAD, or, rather, vegetation structure, seem more certain. Although shelter coefficients observed in other studies refer to the average drag coefficients of whole trees, one could expect the same tendency for the upper and lower layers of a canopy. This is also indicative of the results of Kerzenmacher and Gardiner (1998), who applied an inversion method on data from a spruce forest and obtained a  $C_D = 0.2$  for the stem region (below 8 m) and a  $C_D = 0.1$  for the crown region (above 8 m), i.e. a  $P_m$  of 2. Reasons for the absence of the shelter effect in our study could be: (i) a different relationship between the mean wind speed and Reynolds stress in the upper layer and the lower layer of the canopy; (ii) the fact that the roughness of the vegetation elements is much higher in the crown space and dominates the absorption of momentum; and (iii) the circumstance that the shelter effect is already included in the laser derived PAD values (i.e. the PAD in the dense crown space is underestimated by the laser scanning measurements). The latter assumption is supported by a remaining dependence of the  $C_D$  on PAD. However, the PAD profile of this study is comparable to those of other studies (Halldin and Lindroth 1986), and an increasing PAD of the crown space decreases the derived  $C_D$ , which is already small. Therefore, we tend to assume that the second reason is the most important.

As the dependence of  $C_D$  on PAD for almost all wind sectors shows a similar behaviour, we do recommend parameterising the local drag coefficient  $C_{D,l}$  in the form of  $C_{D,l} = C_D \cdot \text{PAD}^n$ .

## Summary and conclusions

Terrestrial laser scanning is an efficient tool to obtain vegetation models with high spatial resolution. The

application of the Beer–Lambert–Bouguer law is designed for media with low molar absorptivity and is not necessarily applicable in dense forest canopies. A method was suggested that produced more robust results in a numerical test performed on an artificial stand.

Using the derived PAD distribution and multi-level high-frequency wind velocity measurements, the momentum absorption of the forest stand was investigated. Two different experiments were carried out in 2007 and 2008. Despite the different periods in time and changes in sensor positions, the calculated local drag areas reveal conforming patterns and affirm repeatability.

Analysing the wind speed dependence of the local drag area, using different velocity scales, the findings of Cescatti and Marcolla (2004) could be affirmed. Using  $\overline{|U|u}$  instead of  $\bar{u}^2$  as a velocity scale, remarkably reduces the dependence of  $J$  on wind speed and its scatter. These results emphasise the importance of gusts. However, wind speed dependences or streamlining could not be observed for all wind directions. Thus, edge effects, i.e. influences of a local pressure gradients and advective terms on the momentum balance, have to be considered.

A shelter effect was not observed. Instead, the calculated profiles of drag coefficients revealed an increasing trend of  $C_D$  with PAD. The strength of this dependence changes with wind direction, but shows the same pattern for directions with a fetch of 4 *h* as for those with a fetch of more than 10 *h*. Thus, the observed dependence on PAD could most likely be attributed to specific plant structures. Consequently, height-averaged drag coefficients also show a strong dependence on wind direction. Values for the vegetation around tower HM range from 0.1 to 0.4.

We conclude that the derived  $C_D$  reveal high spatial variability, which is partly explained by the laser derived vegetation model. Iterative investigations combining results from measurements and models will probably explain more of the uncertainty in the results.

**Acknowledgments** This study was supported by the ‘Deutsche Forschungsgemeinschaft’ (DFG SPP 1276 *MetStröm*) within the project ‘Turbulent Exchange processes between Forested areas and the Atmosphere’ (Grant BE 1721). We thank Dr. Christian Feigenwinter and Dr. Roland Vogt (University of Basel) for their logistical and scientific support and the technical staff of the Institute of Hydrology and Meteorology of the TUD. The authors would also like to thank Faro Europe GmbH for providing the laser scanner.

## References

- Amiro BD (1990) Drag coefficients and turbulence spectra within three boreal forest canopies. *Bound-Layer Meteorol* 52:227–246
- Arya SP (2001) Introduction to micrometeorology. Academic Press, London

- Aschoff T, Spiecker H (2004) Algorithms for the automatic detection of trees in laser scanner data. In: Thies M, Koch B, Spiecker H, Weinacker H (eds) International society of photogrammetry and remote sensing, Freiburg, pp 66–70
- Aschoff T, Holderied M, Spiecker H (2006) Forstliche Maßnahmen zur Verbesserung von Jagdlebensräumen von Fledermäusen. In: Luhmann T, Müller C (eds) Photogrammetrie—Laserscanning—optische 3D-Messtechnik. Beiträge Oldenburger 3D-Tage 2006. Verlag Herbert Eichmann, Heidelberg, pp 280–287
- Aubinet M, Heinesch B, Bernhofer C, Canepa E, Lindroth A, Montagnani L, Rebmann C, Sedlak P, van Gorsel E (2010) Direct advection measurements do not help to solve the nighttime CO<sub>2</sub> closure problem: evidence from three different forests. *Agric For Meteorol* 150:655–664
- Ayotte KW, Finnigan JJ, Raupach MR (1999) A second-order closure for neutrally stratified vegetative canopy flows. *Bound-Layer Meteorol* 90:189–216
- Bienert A, Queck R, Schmidt A, Bernhofer C, Maas H-G (2010) Voxel space analysis of terrestrial laser scans in forests for wind field modelling. *IAPRS XXXVIII(5)*:92–97
- Brunet Y, Finnigan JJ, Raupach MR (1994) A wind tunnel study of air flow in waving wheat: single-point velocity statistics. *Bound-Layer Meteorol* 70:95–132
- Cava D, Katul GG (2008) Spectral short-circuiting and wake production within the canopy trunk space of an alpine hardwood forest. *Bound-Layer Meteorol* 126:415–431
- Cescatti A, Marcolla B (2004) Drag coefficient and turbulence intensity in conifer canopies. *Agric For Meteorol* 121:197–206
- Coppin PA, Raupach MR, Legg BJ (1986) Experiments on scalar dispersion within a model plant canopy part II: an elevated plane source. *Bound-Layer Meteorol* 35:167–191
- de Langre E (2008) Effects of wind on plants. *Annu Rev Fluid Mech* 40:141–168
- Dupont S, Bonnefond J-M, Irvine MR, Lamaud E, Brunet Y (2011) Long-distance edge effects in a pine forest with a deep and sparse trunk space: in situ and numerical experiments. *Agric For Meteorol* 151:328–344
- Feigenwinter C, Bernhofer C, Vogt R (2004) The influence of advection on the short term CO<sub>2</sub>-budget in and above a forest canopy. *Bound-Layer Meteorol* 113:201–224
- Finnigan JJ (2000) Turbulence in plant canopies. *Annu Rev Fluid Mech* 32:519–571
- Frank C, Ruck B (2008) Numerical study of the airflow over forest clearings. *Forestry* 81:1–19
- Gorte B, Pfeifer N (2004) Structuring laser-scanned trees using 3D mathematical morphology. In Istanbul, Turkey, pp 929–933
- Groß G (1993) Numerical simulation of canopy flows. Springer, New York
- Grünwald T, Bernhofer C (2007) A decade of carbon, water and energy flux measurements of an old spruce forest at the Anchor Station Tharandt. *Tellus B* 59:387–396
- Halldin S, Lindroth A (1986) Pine forest microclimate simulation using different diffusivities. *Bound-Layer Meteorol* 35:103–123
- Hasager CB, Jensen NO (1999) Surface-flux aggregation in heterogeneous terrain. *Q J R Meteorol Soc* 125:2075–2102
- Henning JG, Radtke PJ (2006) Detailed stem measurements of standing trees from ground-based scanning lidar. *For Sci* 52: 67–80
- Kaimal JC, Finnigan JJ (1994) Atmospheric boundary layer flows: their structure and measurement. Oxford University Press, Oxford
- Kerzenmacher T, Gardiner B (1998) A mathematical model to describe the dynamic response of a spruce tree to the wind. *Trees* 12:385–394
- Koizumi A, Motoyama J-i, Sawata K, Sasaki Y, Hirai T (2010) Evaluation of drag coefficients of poplar-tree crowns by a field test method. *J Wood Sci* 56:189–193
- Kraus K, Pfeifer N (2001) Advanced DTM generation from LIDAR data. *IAPRS* 34:23–30
- Landsberg JJ, Thom AS (1971) Aerodynamic properties of a plant of complex structure. *Q J R Meteorol Soc* 97:565–570
- Lefsky M, McHale M (2008) Volume estimates of trees with complex architecture from terrestrial laser scanning. *J Appl Remote Sens* 2(1):1–19
- Li ZJ, Miller DR, Lin JD (1985) A first-order closure scheme to describe counter-gradient momentum transport in plant canopies. *Bound-Layer Meteorol* 33:77–83
- Maas H-G, Bienert A, Scheller S, Keane E (2008) Automatic forest inventory parameter determination from terrestrial laser scanner data. *Int J Remote Sens* 29:1579–1593
- Mahrt L, Vickers D, Sun J, Jensen NO, Allen H, Pardyjak E, Fernando H (2001) Determination of the surface drag coefficient. *Bound-Layer Meteorol* 99:249–276
- Marcolla B, Pitacco A, Cescatti A (2003) Canopy architecture and turbulence structure in a coniferous forest. *Bound-Layer Meteorol* 108:39–59
- Massman WJ (1987) A comparative study of some mathematical models of the mean wind structure and aerodynamic drag of plant canopies. *Bound-Layer Meteorol* 40:179–197
- Massman WJ (1997) An analytical one-dimensional model of momentum transfer by vegetation of arbitrary structure. *Bound-Layer Meteorol* 83:407–421
- Monteith JL, Unsworth MH (2008) Principles of environmental physics. Academic Press, London
- Pfeifer N, Winterhalder D (2004) Modelling of tree cross sections from terrestrial laser scanning data with free-form curves. *IAPRS XXXVI—8/W2*:76–81
- Pinard JDJ-P, Wilson JD (2001) First- and second-order closure models for wind in a plant canopy. *J Appl Meteorol* 40: 1762–1768
- Queck R, Bernhofer C (2010) Constructing wind profiles in forests from limited measurements of wind and vegetation structure. *Agric For Meteorol* 150:724–735
- Raupach MR, Shaw RH (1982) Averaging procedures for flow within vegetation canopies. *Bound-Layer Meteorol* 22:79–90
- Raupach MR, Thom AS (1981) Turbulence in and above plant canopies. *Annu Rev Fluid Mech* 13:97–129
- Shaw RH, Schumann U (1992) Large-eddy simulation of turbulent flow above and within a forest. *Bound-Layer Meteorol* 61:47–64
- Sogachev A, Panferov O (2006) Modification of two-equation models to account for plant drag. *Bound-Layer Meteorol* 121:229–266
- Stewart JB, Thom AS (1973) Energy budgets in pine forest. *Q J R Meteorol Soc* 99:154–170
- Thom AS (1971) Momentum absorption by vegetation. *Q J R Meteorol Soc* 97:414–428
- Vosselman G, Maas H-G (2010) Airborne and terrestrial laser scanning. Whittles Publishing, Dunbeath, Scotland, UK
- Wilson NR, Shaw RH (1977) A higher order closure model for canopy flow. *J Appl Meteorol* 16:1197–1205
- Wood CJ (1995) Understanding wind forces on trees. In: Coutts MP, Grace J (eds) Wind and trees. Cambridge University Press, Cambridge, pp 133–164
- Yang B, Raupach MR, Shaw RH, Paw U KT, Morse A (2006) Large-eddy simulation of turbulent flow across a forest edge. Part I: flow statistics. *Bound-Layer Meteorol* 120:377–412